Direct Growth of Carbon Nanofibers to Generate a 3D Porous Platform on a Metal Contact to Enable an Oxygen Reduction Reaction

David Pan,[†] Matthew Ombaba,[†] Zhi-You Zhou,[‡,§] Yang Liu,[†] Shaowei Chen, and Jennifer Lu[†,*]

[†]School of Engineering, University of California, 5200 N. Lake Road, Merced, California 95343, United States, [‡]Department of Chemistry and Biochemistry, University of California, 1156 High Street, Santa Cruz, California 95064, United States, and [§]State Key Laboratory of Physical Chemistry of Solid Surfaces, Department of Chemistry, College of Chemistry and Chemical Engineering, Xiamen University, Xiamen 361005, China

ABSTRACT For carbon nanotube-based electronics to achieve their full performance potential, it is imperative to minimize the contact resistance between macroscale metal contacts and the carbon nanotube (CNT) nanoelectrodes. We have developed a three-dimensional electrode platform that consists of carbon nanofibers (CNFs) that are directly grown on a metal contact, such as copper (Cu). Carbon nanofiber morphology can be tailored by adjusting the annealing time of a thin electrochemically deposited nickel catalyst layer on copper. We demonstrate that increasing the annealing time increases the amount of copper infused into the nickel catalyst layer. This reduces the carbon deposition rate, and consequently a more well-defined CNF 3D architecture can be fabricated. This direct growth of CNFs on a Cu substrate yields an excellent electron transfer pathway, with contact resistance between CNFs and Cu being comparable to that of a Cu—Cu interface. Furthermore, the excellent bonding strength between CNFs and Cu can be maintained over prolonged periods of ultrasonication. The porous 3D platform affixed with intertwined CNFs allows facile surface functionalization. Using a simple solution soaking procedure, the CNF surface has been successfully functionalized with iron(II) phthalocyanine (FePc). FePc functionalized CNFs exhibit excellent oxygen reduction capability, equivalent to platinum—carbon electrodes. This result demonstrates the technological promise of this new 3D electrode platform that can be exploited in other applications that include sensing, battery, and supercapacitors.

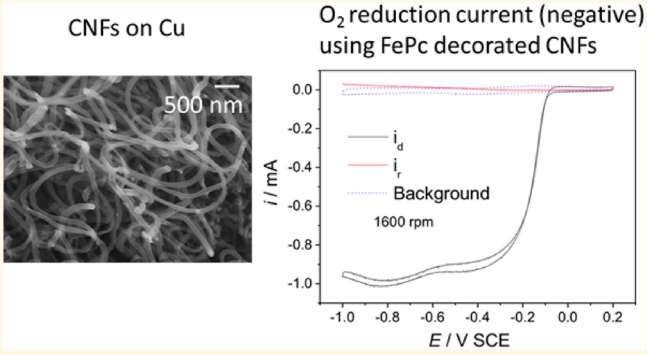

KEYWORDS: carbon nanofibers · nanoscale electrodes · oxygen reduction reaction · direct growth · supercapacitors · fuel cells · 3D electrode platform

Carbon nanotubes (CNTs) and carbon nanofibers (CNFs) are the most lightweight electrically conductive materials. They have excellent electrical conductivity[1] ranging from 10^{-5} to 10^{-3} Ω·m and 10^{-7} to 10^{-5} Ω·m for nanofibers[2,3] and nanotubes,[1,4−7] respectively. In addition, they possess extremely large surface areas that can interact with or anchor/adsorb functional ions and other molecules. With their excellent thermal and chemical stabilities and superb mechanical integrity, 1D carbon materials have been touted as ideal nanoelectrode materials for sensors,[8,9] energy storage,[10−14] and energy conversion.[15−21] In the aforementioned applications and other related electronic technologies, the electrical conductance across the junction between the CNTs and metal electrodes is a critical factor that determines the performance.

Over the years, it has been demonstrated that the direct growth of 1D carbon nanomaterials on metallic substrates creates a superb direct electron transfer pathway. In 2006, Talapatra *et al.* successfully grew high-quality CNTs on Inconel rods.[22] In that study, Inconel 600 (nickel with 17% chromium and 10% iron) served as a catalyst as well as the macroscopic electrode. The CNT—Inconel interface exhibits good electrical contact and can be directly used as an electrode for the supercapacitor application or as a

* Address correspondence to jlu5@ucmerced.edu.

Received for review August 26, 2012 and accepted November 21, 2012.

Published online November 21, 2012
10.1021/nn303910w

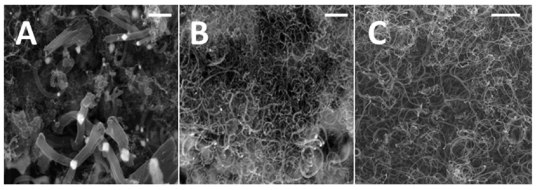

Figure 1. Effect of annealing time on CNF morphology. Scale bar is 3 μm. Prior to growth, the Ni-coated Cu substrates were annealed at (A) 30, (B) 35, and (C) 50 min.

robust field emitter, without any postgrowth processing. However, Inconel is relatively expensive and has poor electrical conductivity (1.03×10^{-3} Ω·m) compared to copper (1.7×10^{-8} Ω·m). More recently, Lahiri *et al.* synthesized CNTs on a copper current collector using a sputtered titanium carbide thin film as a catalytic layer.[11] By employing this CNT–Cu system as an anode in Li–ion cells, significant performance enhancement was observed. This improvement was attributed to the strong bonding of the CNTs to the substrate. However, this high vacuum processing cannot be used to form a conformable coating on nonflat surfaces.

Catalysts are critical for the formation and properties of 1D nanomaterials. Nickel (Ni) and iron (Fe) have been regarded as excellent catalytic systems[23,24] for the growth of 1D carbon nanomaterials. However, they have poor adhesion to copper (Cu). Consequently, chromium, aluminum, and titanium nitride have been used as adhesion promoters between catalysts and the Cu[23–28] substrate. The adhesion layer is often applied onto the Cu substrate by either electron beam evaporation or sputtering techniques. Herein we report a facile approach of direct growth on a copper substrate of any shape without the use of a buffer layer. A Ni catalyst layer was deposited on Cu wires *via* electroplating, to facilitate conformal growth of CNFs on their surfaces. The 3D CNFs' morphology, thickness, and diameter were tuned by a simple annealing process which adjusts the catalyst activity by interdiffusion of Cu into the Ni catalyst layer.

The electrodes, as grown, show low electrical contact resistance between Cu and the grown CNFs and remain attached even after 1 h of sonication at 40 kHz with a power of 135 W. This electrode structure, consisting of porous 1D carbon nanomaterials affixed on the metallic current collector, allows for solution and vapor-based CNF surface functionalization processes. To demonstrate the practical utility of these electrodes, we successfully functionalized CNF surfaces with iron phthalocyanine (FePc) molecules to impart oxygen reduction reaction (ORR) capability. Owing to the excellent electron transfer pathway between FePc–CNFs and CNF to the underlying metal contact, the functionalized electrode exhibited electrocatalytic activity, similar to Pt for the oxygen reduction reaction. This facile fabrication method of generating a porous electrode with tunable architecture will promote the use of

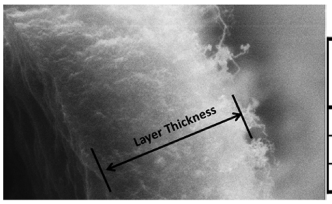

Annealing Time (min)	CNF Layer Thickness (μm)
30	16.5
35	10.5
50	3.6

Figure 2. A typical cross-sectional SEM image of CNFs demonstrating the variations in CNF layer thickness as a function of catalyst annealing time. Other parameters in the growth recipe were kept constant for all samples.

1D carbon materials for a variety of electronic-related applications by offering a morphologically controlled 3D conductive scaffold with excellent electron transfer across 1D carbon nanomaterials and macroscopic metal contact simultaneously for different applications.

RESULTS AND DISCUSSION

Annealing effect. Cu can grow 1D carbon nanomaterials but requires a higher growth temperature, typically over 800 °C due to low carbon solubility and poor graphitization ability[23–25,29–31] in Cu. It is known that Ni is an excellent catalyst due to its finite solubility with carbon and great tendency to promote graphitization.[24,25,32,33] Without Ni, there is no growth on Cu wires at 650 °C. Increasing the annealing time will increase Cu and Ni interdiffusion since they are mutually soluble at all concentrations, as evidenced by their binary phase diagram.[34] The net result is a "dilution" of Ni's catalytic properties because Cu has a lower melting point than Ni, thus the Cu–Ni alloy will decrease the rate of carbon incorporation. Figure 1 is a set of SEM micrographs of CNFs grown on Cu using the same catalytic system but under different annealing conditions. The catalyst seed is highly visible at the CNF tip with roughly the same diameter as the CNF. The presence of the catalyst at the tip indicates tip-based growth and also implies that there is a direct contact between the roots of the CNFs and the Cu substrate. By increasing the thermal annealing time, that is, more Cu interdiffusion into the Ni catalyst layer, CNFs become more distinguishable. The thickness of the CNF layer is reduced from 10 to 4 μm with an increased annealing time from 35 to 50 min (as displayed in the table in Figure 2) while the CNF diameter is reduced down to 100 nm. This result is in good agreement with previously published results[35,36] which observed that increasing the Cu content in catalytic systems reduces the carbon deposition rate, leading to the formation of smaller CNFs and CNTs.

Raman spectroscopy of the CNFs was used to identify and assess the quality of the CNFs as shown in Supporting Information, Figure S2. The spectra exhibit the G-band peak in the vicinity of 1590 cm^{-1} associated with the graphitic structure of carbon as well as the D-band peak at 1380 cm^{-1} that is normally ascribed to defects therein. Upon estimating the ratio

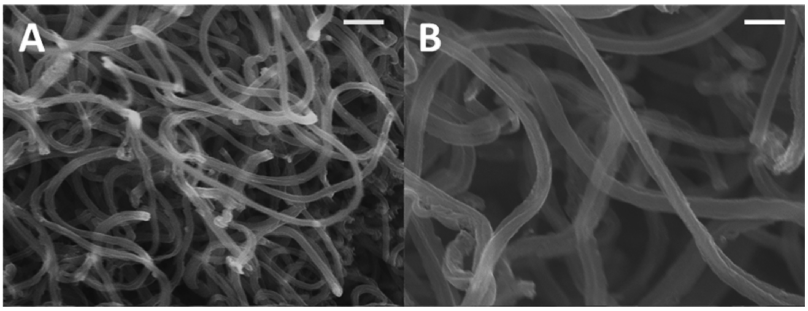

Figure 3. High magnification of CNFs. Shown are micrographs from catalysts annealed for 50 min. Scale bar: (A) 500 nm, (B) 250 nm.

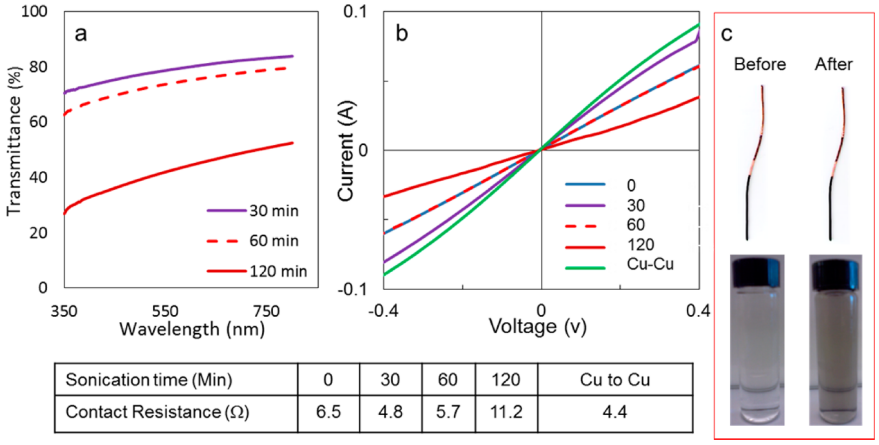

Sonication time (Min)	0	30	60	120	Cu to Cu
Contact Resistance (Ω)	6.5	4.8	5.7	11.2	4.4

Figure 4. a) UV−vis transmission spectra of ethanol solutions after sonication of CNF of Cu substrates. (b) *I*−*V* curves of the CNF−Cu interface after varied sonication durations. (c) Picture of CNF on Cu substrate before and after sonication for 60 min.

of the G and D band peaks of the grown CNFs, it was noted that the defects or the distributions thereof were similar irrespective of the annealing time, given that the ratios between the bands were more or less the same. Despite the negativity associated with defects within the CNFs, their presence in all samples could be beneficial in uniform postgrowth functionalization[8,37,38] with surface dopants and other associated functional entities.

Figure 3 is a set of high magnification micrographs showing that distinct and individual CNFs are on the order of 100 nm in diameter using a Ni-on-Cu catalyst system annealed for approximately 50 min. In addition, the CNFs exhibit a well-defined porous structure. This set of wires was used for adhesion testing and electrical conductivity simultaneously. Furthermore, they were subsequently functionalized and used for ORR studies.

Adhesion and Conductivity Study. To evaluate the CNF adhesion to the underlying Cu substrate, the CNF/Cu samples were immersed in ethanol and then subjected to sonication over different durations. UV−visible spectrometry was used to evaluate the absorption of the resultant solutions as shown in Figure 4a. Longer sonication times resulted in higher optical absorption of the solution. Photographs of a single CNF/Cu sample before and after sonication for 1 h as well as their respective ethanol solutions are shown in Figure 4c. After sonication of the substrate, the vast majority of CNFs remained bonded onto the Cu substrate. SEM inspection of the black solid that was removed after sonication indicates that it did not contain a significant quantity of CNFs. It is believed that the black material is amorphous carbon particulates that were not bound to the Cu substrate. Contact resistance measurements between CNFs and Cu did not increase after sonication; a testament to the fact that there is a superbly strong CNF to Cu bond.

I−V curves were measured to examine electrical charge transport across the CNF−Cu interface, as shown in Figure 4b, using a two-probe contact resistance protocol whereby a potential sweep was applied (−0.4 to 0.4 V) and the resultant current was recorded. The distance between probes was kept constant as depicted in Supporting Information, Figure S3a. The straight *I*−*V* curves through the origin are indicative of ohmic characteristics between CNFs and Cu. As shown in the corresponding table in Figure 4, the electrical contact resistance between CNFs and the underlying Cu substrate was low, approximately 4 Ω. This was found to be comparable to that of Cu to Cu. This value was much lower than contact resistances of CNFs physically immobilized on metals, which typically have a contact resistance that ranges from 1 to 300 KΩ.[39,40] Such low resistance across the metal/CNF interface has

only been demonstrated on ion beam bombarded samples.[39,41] The excellent conductivity between CNFs and Cu is thought to be due to a seamless integration of CNFs to Cu substrate. From the SEM micrographs in Figures 1 and 2, the most probable CNF formation mechanism was *via* tip-growth, similar to Boellaard's finding.[35] Therefore it is hypothesized that the open end CNT−Cu bond at the root of the fiber was the dominant junction as shown in Supporting Information, Figure S3b. It must be stated that a monolithic integration of macroscopic electrodes with nanoscale carbon electrodes is necessary in order to have efficient electron transfer.[42]

Oxygen Reduction Reaction. Electrocatalytic reduction of oxygen to water is a process of great importance in fuel cell technology. Research toward non-noble metal based catalysis is a field of intense research.[18,43,44] Metallophthalocyanines (MPc), such as FePc, NiPc, and CoPc have continued to show great potential in the cathodic reduction of oxygen.[45−52] To demonstrate the technological potential of this simple 3D electrode platform, we performed solution-based functionalization to immobilize FePc molecules. SEM micrographs of the CNFs before and after functionalization (Figure 5) show that minimal agglomeration occurred, an attestation that they retained their high surface area. This is due to the combination of a strong interface between CNFs and Cu as well as the relatively large fiber diameter that imparted individual fiber rigidity. Such a configuration enabled solution functionalization of the CNF surfaces with minimal aggregation to render the desired properties. In stark contrast, conventionally functionalized electrodes prepared by mixing either carbon powders or CNTs with either catalyst or redox active centers in solution together with binder lose a significant percentage of their surface area due to the agglomeration of carbon materials.

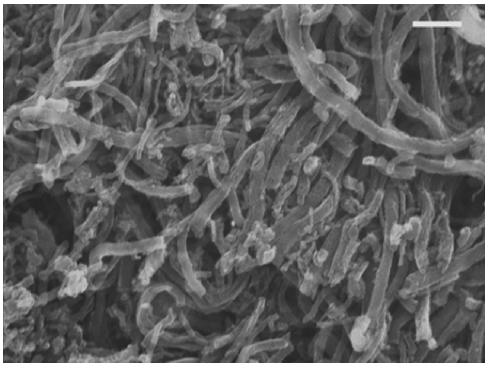

Figure 5. Micrographs of functionalized CNFs. The grown CNFs were functionalized by soaking in an iron(II) phthalocyanine solution to enhance electrocatalytic activity. Scale bar is 500 nm.

Cyclic voltammetry (CV) was used to evaluate the ORR activity of a Cu wire, a CNF/Cu sample, and a FePc functionalized CNF/Cu electrode under both N_2 and O_2 rich electrolytic solutions. As shown in Figure 6a, the cyclic voltammograms of the Cu wire exhibited two oxidative peaks during the anodic sweep, centered on −0.3 and −0.15 V. In the subsequent cathodic sweep, two reductive peaks centered at −0.32 and −0.75 V were noted. The two pairs of peaks are attributed to the two-stage redox processes associated with Cu.[53] The CVs of the other two samples exhibited larger current response in addition to the Cu redox processes. As expected, no O_2 reductive activity was noted by the three samples in a N_2-rich environment. However, upon repeating the same experiments in an O_2-rich electrolytic solution, both the CNF/Cu electrode as well as the electrode infused with FePc exhibited ORR activity, as shown in Figure 6b. This is in good agreement with other published results,[17] implying that 1D carbon nanomaterials exhibit electrocatalytic activity. The enhanced ORR activity, improved current gain and low on-set potential of the FePc functionalized CNFs are thought to be due to the combination of a 3D porous structure which provided an extremely large surface area for effective incorporation of FePc, and the facile electron transfer between catalyst, 3D carbon electrode, and current collector.

The catalytic activity of FePc-functionalized CNFs was also evaluated by rotating disk electrode (RDE)

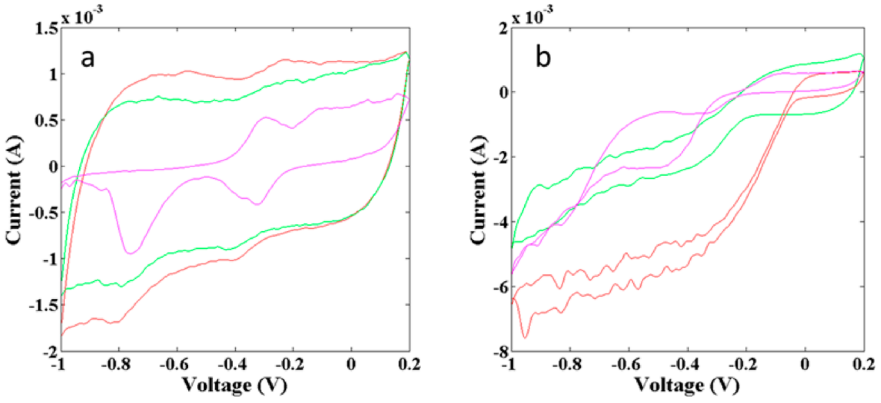

Figure 6. Cyclic voltammograms in (a) N_2 saturated 0.1 M NaOH and in (b) saturated O_2: Cu wire (purple), FePc functionalized samples (red), as grown samples (green) at the scan rate of 50 mV s^{-1}.

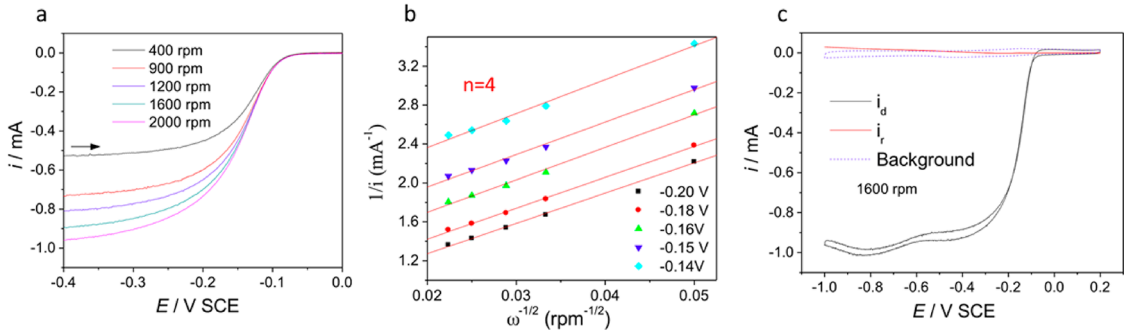

Figure 7. (a) Polarization curves of FePc functionalized CNFs in O_2-saturated 0.1 M NaOH (scan rate, 10 mV s^{-1}; room temperature) and (b) the corresponding Koutecky–Levich plot; (c) RRDE measurement of oxygen reduction (negative current) and hydrogen peroxide oxidation (positive current) using the FePc-decorated CNFs at 1600 rpm in O_2-saturated 0.1 M NaOH: (i_d) disk current; (i_r) ring current (scan rate, 10 mV s^{-1}; room temperature).

voltammetry. Figure 7a shows the polarization curves at different rotation rates and the corresponding Koutecky–Levich plot in Figure 7b. The onset potential of the oxygen reduction potential was approximately 80 mV, comparable to the value obtained from the Pt/C reference.[20] Slopes of the experimental data in the Koutecky–Levich plot at each rotation speed are very close to 4. This indicates 4 electron reduction of O_2 in good agreement with literature.[50]

It is common knowledge that the indirect or peroxide pathway of oxygen reduction involves the formation of peroxide (H_2O_2) as an intermediate, where oxygen is first reduced to H_2O_2 and then further reduction of the H_2O_2 to water occurs *via* a 2-electron process, whereas the direct reduction to water is *via* the 4-electron process. Peroxide is conveniently detected electrochemically using a gold rotating ring-disk electrode (RRDE). The Koutecky–Levich plot (calculations available in the Supporting Information, Figure S4) using the result from the RRDE measurement is shown in Figure 7b. It demonstrates that the reduction reaction of our FePc–CNF system occurs through a 3.95 electron pathway with minimal hydrogen peroxide production of 2.5%. This indicates that the newly fabricated 3D electrode with adsorbed FePc molecules is highly effective for the reduction of oxygen. This result also indicates that the 3D electrodes provide ohmic contact with 1D nanomaterials and that 3D electrodes made of CNFs are excellent conductive scaffolds for surface functionalization. Supporting Information, Figure S5 contains two XPS core-level spectra of Pt 4f obtained from our FePc-CNF system. XPS analysis shows no trace of platinum.

CONCLUSION

We have demonstrated a facile process to fabricate 3D CNF-based electrodes directly on a metal contact. Due to the ultralow contact resistance of the as grown CNFs with metals and strong bond strength between CNFs and the metal contact, solution functionalization of the CNF surfaces for desired properties can be readily achieved. FePc-decorated carbon surfaces offer excellent electrocatalytic activity and have the potential to be used as cathode material for ORR in fuel cell technologies. Many applications require the growth of nanoelectrodes directly on a current collector to maximize total surface area while ensuring low current loss such as sensors, batteries, or supercapacitors. By employing direct growth, most post-processing steps can be eliminated. This 3D electrode design protocol eliminates the use of binders, thus maintaining the large surface area offered by the CNF platform. By electroplating a thin catalyst layer, CNFs can be grown on electrodes of any type and shape. Furthermore, by tailoring the catalyst's properties using a simple thermal annealing, growth of CNFs with controlled morphologies can be achieved. This new fabrication method to generate a well-defined 3D porous electrode platform with morphology control provides an enabling conductive scaffold for energy storage, energy conversion, and sensing.

METHODS

Catalyst and Substrate Preparation. Eighteen AWG Cu wire (Fisher Scientific) was polished using emery paper to mechanically roughen the surface. It was then chemically treated with nitric acid and subsequently hydrochloric acid to provide a clean surface. Photographs at various stages of cleaning were taken using an upright microscope (Olympus BX51) as indicated in the Supporting Information, Figure S1. A nickel thin film was electroplated onto a copper wire substrate from a 0.02 M nickel salt solution composed of nickel(II) nitrate and nickel(II) chloride (Sigma-Aldrich) using a galvanostatic current of 0.3 mA for 3 min (Princeton Applied Research model 263a) with a 3-electrode setup.

Chemical Vapor Growth. The copper wire substrate was placed in a tube furnace and annealed in an argon/hydrogen environment at 600 °C to ensure that both Ni and Cu were in their reduced state. Ethylene gas was introduced into the chamber at a rate of 50 sccm at 650 °C for 10 min during the growth step. After the growth, both hydrogen and ethylene gases were turned off and substrates subsequently cooled in vacuum to 300 °C and then in argon to room temperature.

Growth Characterization and Interface Study. The synthesized CNFs on Cu samples were characterized using a Philips XL30 FEG and Hitachi S-4100 scanning electron microscope (SEM). Adhesion studies of the CNFs on the Cu were performed by sonication of the samples in ethanol using a Branson ultrasonicator at 40 kHz with a power of 135 W. Optical images of CNF/Cu samples were taken using a hand-held digital camera before and after sonication.

I−*V* curves were obtained using a Hewlett-Packard 4145B semiconductor parameter analyzer to study contact resistance between Cu-to-Cu and Cu-to-CNFs before and after sonication. To ensure good contact with Cu probes, the probes were cleaned each time before measurement.

UV−vis spectroscopic analysis study of ethanol solutions after sonication was performed using a Perkin-Elmer Lambda UV−vis spectrophotometer to further study the extent of CNF adhesion on Cu.

Raman spectra were obtained using a Renishaw RM2000 system operating at 632.8 nm with a power of 2 mW to observe fiber chemical changes as a function of various growth conditions.

Functionalization, Oxygen Reduction Study, and Postmeasurement Characterization. FePc solution was prepared by dissolving FePc (TCI America) in tetrahydrofuran (Sigma-Aldrich). The CNFs on Cu substrates were functionalized by soaking them in 0.02 M FePc solution for 3 days. Excess iron was removed by rinsing in tetrahydrofuran. SEM was used to characterize the change in morphology. CNF/Cu samples were placed in a 0.1 M sodium hydroxide solution purged with pure nitrogen and oxygen gas. Using a reference electrode of saturated potassium chloride Ag/AgCl and Pt counter electrode, the oxygen reduction reaction was studied by cyclic voltammetry obtained using a potentiostat (Princeton Applied Research model 263a).

To better understand the kinetics of the oxygen reduction from our CNFs, we employed the rotating disk electrode (RDE) technique which eliminates mass transport problems. The functionalized CNFs, 50 mg by weight, were scraped from Cu wires and mixed with a 0.05% Nafion binder before depositing onto a rotating graphite disk electrode (0.070 cm^2). The RDE experiment was run with a Pt counter electrode and Ag/AgCl reference electrode. The rotating ring-disk electrode method was subsequently used to detect the amount of peroxide generated electrochemically using a gold ring electrode with Ag/AgCl as the reference electrode.

X-ray photoelectron spectra (XPS) of functionalized wires were obtained from an upgraded PHI-5000C ESCA system (Perkin-Elmer). The monochromatic Mg Kα with photon energy of 1253.6 eV was selected as the X-ray source. FePc functionalized CNFs were removed from the Cu wire and placed onto a glass slide for analysis.

Conflict of Interest: The authors declare no competing financial interest.

Acknowledgment. We thank the National Science Foundation and DARPA for financial support. We are grateful to the J. Zhang group at University of California, Santa Cruz for providing Raman spectroscopy analysis and CC Wang group at Fudan University for help with the XPS analysis.

Supporting Information Available: Optical micrographs of substrates, Raman spectra, contact resistance measurement diagram, oxygen reduction pathway calculations, and XPS spectra. This material is available free of charge *via* the Internet at http://pubs.acs.org.

REFERENCES AND NOTES

1. Zhao, Y.; Wei, J.; Vajtai, R.; Ajayan, P. M.; Barrera, E. V. Iodine Doped Carbon Nanotube Cables Exceeding Specific Electrical Conductivity of Metals. *Sci. Rep.* **2011**, *1*, 83.
2. McCreery, R. L. Advanced Carbon Electrode Materials for Molecular Electrochemistry. *Chem. Rev.* **2008**, *108*, 2646–2687.
3. Tibbetts, G.; Lake, M.; Strong, K.; Rice, B. A Review of the Fabrication and Properties of Vapor-Grown Carbon Nanofiber/Polymer Composites. *Compos. Sci. Technol.* **2007**, *67*, 1709–1718.
4. Liu, K.; Sun, Y.; Lin, X.; Zhou, R.; Wang, J.; Fan, S.; Jiang, K. Scratch-Resistant, Highly Conductive, and High-Strength Carbon Nanotube-Based Composite Yarns. *ACS Nano* **2010**, *4*, 5827–5834.
5. Zhong, X.-H.; Li, Y.-L.; Liu, Y.-K.; Qiao, X.-H.; Feng, Y.; Liang, J.; Jin, J.; Zhu, L.; Hou, F.; Li, J.-Y. Continuous Multilayered Carbon Nanotube Yarns. *Adv. Mater. (Weinheim, Germany)* **2010**, *22*, 692–696.
6. Zhang, M.; Atkinson, K. R.; Baughman, R. H. Multifunctional Carbon Nanotube Yarns by Downsizing an Ancient Technology. *Science* **2004**, *306*, 1358–1361.
7. Zhang, X.; Li, Q.; Tu, Y.; Li, Y.; Coulter, J. Y.; Zheng, L.; Zhao, Y.; Jia, Q.; Peterson, D. E.; Zhu, Y. Strong Carbon-Nanotube Fibers Spun from Long Carbon-Nanotube Arrays. *Small* **2007**, *3*, 244–248.
8. Wildgoose, G. G.; Banks, C. E.; Leventis, H. C.; Compton, R. G. Chemically Modified Carbon Nanotubes for Use in Electroanalysis. *Microchim. Acta* **2005**, *152*, 187–214.
9. Wang, J.; Musameh, M. Carbon Nanotube/Teflon Composite Electrochemical Sensors and Biosensors. *Anal. Chem.* **2003**, *75*, 2075–2079.
10. Sivakkumar, S. R.; Kim, D.-W. Polyaniline/Carbon Nanotube Composite Cathode for Rechargeable Lithium Polymer Batteries Assembled with Gel Polymer Electrolyte. *J. Electrochem. Soc.* **2007**, *154*, A134.
11. Lahiri, I.; Oh, S.-W.; Hwang, J. Y.; Cho, S.; Sun, Y.-K.; Banerjee, R.; Choi, W. High Capacity and Excellent Stability of Lithium Ion Battery Anode Using Interface-Controlled Binder-Free Multiwall Carbon Nanotubes Grown on Copper. *ACS Nano* **2010**, *4*, 3440–3446.
12. Ban, C.; Wu, Z.; Gillaspie, D. T.; Chen, L.; Yan, Y.; Blackburn, J. L.; Dillon, A. C. Nanostructured Fe_3O_4/SWNT Electrode: Binder-free and High-Rate Li-Ion Anode. *Adv. Mater. (Weinheim, Ger.)* **2010**, *22*, E145–E149.
13. Lee, S. W.; Yabuuchi, N.; Gallant, B. M.; Chen, S.; Kim, B.-S.; Hammond, P. T.; Shao-Horn, Y. High-Power Lithium Batteries from Functionalized Carbon-Nanotube Electrodes. *Nat. Nanotechnol.* **2010**, *5*, 531–537.
14. Zhou, Y.; Wang, J.; Hu, Y.; O'Hayre, R.; Shao, Z. A Porous $LiFePO_4$ and Carbon Nanotube Composite. *Chem. Commun. (Cambridge, U.K.)* **2010**, *46*, 7151–7153.
15. Bashyam, R.; Zelenay, P. A Class of Non-precious Metal Composite Catalysts for Fuel Cells. *Nature* **2006**, *443*, 63–66.
16. Oh, H.-S.; Oh, J.-G.; Lee, W. H.; Kim, H.-J.; Kim, H. The Influence of the Structural Properties of Carbon on the Oxygen Reduction Reaction of Nitrogen Modified Carbon Based Catalysts. *Int. J. Hydrogen Energy* **2011**, *36*, 8181–8186.
17. Gong, K.; Du, F.; Xia, Z.; Durstock, M.; Dai, L. Nitrogen-Doped Carbon Nanotube Arrays with High Electrocatalytic Activity for Oxygen Reduction. *Science* **2009**, *323*, 760–764.
18. Wang, S.; Yu, D.; Dai, L. Polyelectrolyte Functionalized Carbon Nanotubes as Efficient Metal-Free Electrocatalysts for Oxygen Reduction. *J. Am. Chem. Soc.* **2011**, *133*, 5182–5185.
19. Yang, L.; Jiang, S.; Zhao, Y.; Zhu, L.; Chen, S.; Wang, X.; Wu, Q.; Ma, J.; Ma, Y.; Hu, Z. Boron-Doped Carbon Nanotubes as Metal-Free Electrocatalysts for the Oxygen Reduction Reaction. *Angew. Chem., Int. Ed.* **2011**, 1–6.
20. Lefèvre, M.; Proietti, E.; Jaouen, F.; Dodelet, J.-P. Iron-Based Catalysts with Improved Oxygen Reduction Activity in Polymer Electrolyte Fuel Cells. *Science* **2009**, *324*, 71–74.
21. Gong, K.; Yu, P.; Su, L.; Xiong, S.; Mao, L. Polymer-Assisted Synthesis of Manganese Dioxide/Carbon Nanotube Nanocomposite with Excellent Electrocatalytic Activity toward Reduction of Oxygen. *J. Phys. Chem. C* **2007**, *111*, 1882–1887.
22. Talapatra, S.; Kar, S.; Pal, S. K.; Vajtai, R.; Ci, L.; Victor, P.; Shaijumon, M. M.; Kaur, S.; Nalamasu, O.; Ajayan, P. M. Direct Growth of Aligned Carbon Nanotubes on Bulk Metals. *Nat. Nanotechnol.* **2006**, *1*, 112–116.
23. Deck, C.; Vecchio, K. Prediction of Carbon Nanotube Growth Success by the Analysis of Carbon−Catalyst Binary Phase Diagrams. *Carbon* **2006**, *44*, 267–275.

24. Baker, R. T. K. Catalytic Growth of Carbon Filaments. *Carbon* **1989**, *27*, 315–323.
25. Neupane, S.; Lastres, M.; Chiarella, M.; Li, W.; Su, Q.; Du, G. Synthesis and Field Emission Properties of Vertically Aligned Carbon Nanotube Arrays on Copper. *Carbon* **2012**, *50*, 2641–2650.
26. Park, M.; Cola, B. A.; Siegmund, T.; Xu, J.; Maschmann, M. R.; Fisher, T. S.; Kim, H. Effects of a Carbon Nanotube Layer on Electrical Contact Resistance between Copper Substrates. *Nanotechnology* **2006**, *17*, 2294–2303.
27. Wong, C. P. Synthesis of High-Quality Vertically Aligned Carbon Nanotubes on Bulk Copper Substrate for Thermal Management. *IEEE Trans. Adv. Packag.* **2010**, *33*, 370–376.
28. Dubosc, M.; Casimirius, S.; Besland, M.-P.; Cardinaud, C.; Granier, A.; Duvail, J.-L.; Gohier, A.; Minéa, T.; Arnal, V.; Torres, J. Impact of the Cu-Based Substrates and Catalyst Deposition Techniques on Carbon Nanotube Growth at Low Temperature by PECVD. *Microelectron. Eng.* **2007**, *84*, 2501–2505.
29. Zhou, W.; Han, Z.; Wang, J.; Zhang, Y.; Jin, Z.; Sun, X.; Zhang, Y.; Yan, C.; Li, Y. Copper Catalyzing Growth of Single-walled Carbon Nanotubes on Substrates. *Nano Lett.* **2006**, *6*, 2987–90.
30. Kumar, S.; Levchenko, I.; Keidar, M.; Ostrikov, K. Plasma-Enabled Growth of Separated, Vertically Aligned Copper-Capped Carbon Nanocones on Silicon. *Appl. Phys. Lett.* **2010**, *97*, 151503.
31. Mata, D.; Amaral, M.; Fernandes, A. J. S.; Oliveira, F. J.; Costa, P. M. F. J.; Silva, R. F. Self-Assembled Cones of Aligned Carbon Nanofibers Grown on Wet-Etched Cu Foils. *Carbon* **2011**, *49*, 2181–2196.
32. Chai, Y.; Hazeghi, A.; Takei, K.; Chen, H.-Y.; Chan, P. C. H.; Javey, A.; Wong, H.-S. P. Low-Resistance Electrical Contact to Carbon Nanotubes with Graphitic Interfacial Layer. *IEEE Trans. Electron Devices* **2012**, *59*, 12–19.
33. Yudasaka, M.; Kasuya, Y.; Kokai, F.; Takahashi, K.; Takizawa, M.; Bandow, S.; Iijima, S. Causes of Different Catalytic Activities of Metals in Formation of Single-Wall Carbon Nanotubes. *Appl. Physi. A: Mater. Sci. Process* **2002**, *74*, 377–385.
34. Gupta, K. P. An Expanded Cu–Ni–Sn System (Copper–Nickel–Tin). *J. Phase Equilib.* **2000**, *21*, 479–484.
35. Boellaard, E. The Formation of Filamentous Carbon on Iron and Nickel Catalysts III. Morphology. *J. Catal.* **1985**, *96*, 481–490.
36. Bernardo, C. A.; Alstrup, I.; Rostrup-Nielsen, J. R. Carbon Deposition and Methane Steam Reforming on Silica-Supported Ni-Cu Catalysts. *J. Catal.* **1985**, *96*, 517–534.
37. Lee, S. H.; Lee, D. H.; Lee, W. J.; Kim, S. O. Tailored Assembly of Carbon Nanotubes and Graphene. *Adv. Funct. Mater.* **2011**, *21*, 1338–1354.
38. Pumera, M. The Electrochemistry of Carbon Nanotubes: Fundamentals and Applications. *Chemistry* **2009**, *15*, 4970–4978.
39. Wei, B. Q.; Vajtai, R.; Ajayan, P. M. Reliability and Current Carrying Capacity of Carbon Nanotubes. *Appl. Phys. Lett.* **2001**, *79*, 1172.
40. Tersoff, J. Contact Resistance of Carbon Nanotubes. *Appl. Phys. Lett.* **1999**, *74*, 2122.
41. Tzeng, Y.; Chen, Y.; Liu, C. Electrical Contacts between Carbon-Nanotube Coated Electrodes. *Diamond Relat. Mater.* **2003**, *12*, 774–779.
42. Gao, F.; Qu, J.; Yao, M. Electrical Resistance at Carbon Nanotube/Copper Interfaces: Capped *versus* Open-End Carbon Nanotubes. *Mater. Lett.* **2012**, *82*, 184–187.
43. Wang, S.; Jiang, S. P.; White, T. J.; Guo, J.; Wang, X. Electrocatalytic Activity and Interconnectivity of Pt Nanoparticles on Multiwalled Carbon Nanotubes for Fuel Cells. *J. Phys. Chem. C* **2009**, *113*, 18935–18945.
44. Zhang, J.; Sasaki, K.; Sutter, E.; Adzic, R. R. Stabilization of Platinum Oxygen-Reduction Electrocatalysts Using Gold Clusters. *Science* **2007**, *315*, 220–222.
45. Sehlotho, N.; Nyokong, T. Effects of Ring Substituents on Electrocatalytic Activity of Manganese Phthalocyanines towards the Reduction of Molecular Oxygen. *J. Electroanal. Chem.* **2006**, *595*, 161–167.
46. Obirai, J.; Nyokong, T. Synthesis, Spectral and Electrochemical Characterization of Mercaptopyrimidine-Substituted Cobalt, Manganese and Zn (II) Phthalocyanine Complexes. *Electrochim. Acta* **2005**, *50*, 3296–3304.
47. Jasinski, R. Cobalt Phthalocyanine as a Fuel Cell Cathode. *J. Electrochem. Soc.* **1965**, *112*, 526–528.
48. Jasinski, R. A New Fuel Cell Cathode Catalyst. *Nature* **1964**, *201*, 1212–1213.
49. Kobayashi, N.; Janda, P.; Lever, A. B. P. Cathodic Reduction of Oxygen and Hydrogen Peroxide at Cobalt and Iron Crowned Phthalocyanines Adsorbed on Highly Oriented Pyrolytic Graphite Electrodes. *Inorg. Chem.* **1992**, *31*, 5172–5177.
50. Morozan, A.; Campidelli, S.; Filoramo, A.; Jousselme, B.; Palacin, S. Catalytic Activity of Cobalt and Iron Phthalocyanines or Porphyrins Supported on Different Carbon Nanotubes towards Oxygen Reduction Reaction. *Carbon* **2011**, *49*, 4839–4847.
51. Bezeera, C.; Zhang, L.; Lee, K.; Liu, H.; Marques, A.; Marques, E.; Wang, H.; Zhang, J. A Review of Fe–N/C and Co–N/C Catalysts for the Oxygen Reduction Reaction. *Electrochim. Acta* **2008**, *53*, 4937–4951.
52. Mamuru, S. A.; Ozoemena, K. I.; Fukuda, T.; Kobayashi, N.; Nyokong, T. Studies on the Heterogeneous Electron Transport and Oxygen Reduction Reaction at Metal (Co, Fe) Octabutylsulphonylphthalocyanines Supported on Multi-walled Carbon Nanotube Modified Graphite Electrode. *Electrochim. Acta* **2010**, *55*, 6367–6375.
53. Droog, J. M. M.; Alderliesten, C. A.; Alderliesten, P. T.; Bootsma, G. A. Initial Stages of Anodic Oxidation of Polycrystalline Copper Electrodes in Alkaline Solution. *J. Electroanal. Chem. Interfacial Electrochem.* **1980**, *111*, 61–70.